Available online at www.sciencedirect.com

ScienceDirect

Procedia CIRP 123 (2024) 274–279

www.elsevier.com/locate/procedia

7th CIRP Conference on Surface Integrity

Analytical model to identify crack initiation in machined aluminium parts

G. Ortiz-de-Zarate[a], A. Madariaga[b]*, I. Perez[a], P.J. Arrazola[a]

[a]*Mondragon Unibertsitatea, Engineering Faculty, Loramendi 4, 20500, Arrasate-Mondragon, Spain*
[b]*The University of Manchester, Department of Materials, Oxford Road, M13 9PL, UK*

* Corresponding author. Tel.: 0161 306 6000; *e-mail address:* aitor.madariaga@manchester.ac.uk

Abstract

Thin-walled aluminium components used in the structure of aircrafts are subjected to fatigue loads. Fatigue performance of those components is affected by the surface integrity generated in the last machining step. This paper proposes an analytical model to identify the fatigue crack initiation site considering the surface topography, residual stresses (RS) and mechanical properties induced by machining. To validate the model fatigue samples of aluminium 7050-T7451 were prepared by face milling. Machining-induced RS were measured by hole-drilling and the surface topography of the gauge region of the fatigue samples was characterised using a confocal microscope. Then, uniaxial fatigue tests were done at $R = 0.1$ and subsequently the fracture was analysed. The model predicted nucleation of cracks at the surface when the stress amplitude was above 290 MPa. Fatigue tests done at an amplitude of 350 MPa confirmed crack initiation at the points with the highest stress concentration predicted by the model. By contrast, the cracks were nucleated at the side of the samples when the stress amplitude was below 290 MPa. In fact, compressive RS induced by face milling protected the surface from crack nucleation at lower applied stresses as predicted by the model.

Keywords: surface topography; residual stresses; fatigue; modelling; aluminium alloys

1. Main text

Aircraft manufacturers are seeking for lightweight aerostructures that will enable the reduction of fuel consumption and pollutant emissions. To this end, large thin-walled monolithic aluminium parts are used in the principal structure and load bearing components of the aircraft, mainly because of their high specific strength and good forming properties [1]. The in-service performance of the main structure of the aircraft must be accomplished in the design stage, and particularly the fatigue and corrosion behaviour of thin-walled aluminium parts [2]. These components are manufactured by high-speed machining [3] and their fatigue behaviour is highly affected by its surface integrity in terms of surface topography, residual stresses (RS), micro-hardness and potential microstructural alterations.

Beyond this context several authors have studied the fatigue performance of machined aluminium components and develop fatigue prediction models. Ås et al. [4] conducted a pioneering work. They carried out uniaxial fatigue tests of smooth and rough surfaces of turned aluminium alloy 6082.52-T6. They measured the surface topography, and they included the 2D surface profiles in a Finite Element Model (FEM) to calculate stress concentration factors (Kt) and local stresses. They observed that cracks were nucleated ahead of 10 µm depth when $Kt > 2$ and they suggested the need to add the effect of RS and plasticity to improve their model.

Later, Suratachi et al. [5] did bending fatigue tests of aluminium alloy 7010-T7451 specimens manufactured under seven different milling conditions. For the tested surface conditions, they found the effect of surface topography was more relevant than the influence of RS. Consequently, they

10.1016/j.procir.2024.05.049

used a FEM model to calculate stress concentration factors and include in analytical fatigue prediction models, while RS were excluded from the analysis. They also highlighted the need to establish alternative models to determine stress concentration factors in larger machined surfaces, since FEM with small elements requires significant computational cost.

More recently, Abrough and co-workers [6] performed bending fatigue tests of aluminum alloy 7050-T7451 machined under five different conditions, leading to specimens with surface roughness ranging from height parameter Sa < 0.4 µm to Sa ≈ 5.5 µm. They found a good correlation between Sa and the fatigue limit of the different tested batches. They also developed a FEM of the characterised surface topography to determine local stresses which confirmed that cracks were initiated at high stress locations. They completed their analysis in a subsequent work [7] and added the effect of the size of the machined groove in a probabilistic model to predict the fatigue strength of machined specimens.

Finishing machining conditions usually induce compressive (sub)surface RS in aluminium alloys [8], which could retard or even avoid crack initiation on the surface. The previous works [5-7] found a good correlation between stress concentration factor and fatigue performance, but they did not include the effect of RS. Furthermore, they performed reverse bending fatigue tests which induce the highest applied stresses near the surface and thus minimise the effect of compressive RS typically found in aluminium alloys. This idea was originally supported by Ås et al. [4], who observed most cracks initiating beneath the surface in uniaxial tests, and suggesting the need to include the effect of RS and local plasticity.

This paper is aimed at developing an analytical model to identify the fatigue crack initiation site considering the surface topography, RS and mechanical properties induced by machining. For this purpose, fatigue samples of aluminium alloy 7050-T7451 were obtained by face milling. Machining-induced RS were measured by hole-drilling and the surface topography of the gauge region of the fatigue samples was characterised using a confocal microscope. Then, uniaxial fatigue tests were done at stress ratio R = 0.1 and subsequently the fracture was analysed to identify the crack initiation site. Finally, the experimentally identified and predicted crack initiation site were compared to validate the model.

2. Model to predict crack initiation

The proposed analytical model to predict the fatigue crack initiation site calculates the local stress state taking into account parameters of the surface integrity of the specimen, material's mechanical properties and applied stress. This approach will be first applied to predict the fatigue crack initiation site in aerospace aluminum alloys. In our previous study [2], we did not observe changes in microhardness values from the surface to the bulk in aluminium 7050-T7451 specimens machined by finishing condition. For this reason, it is assumed that the yield stress σ_y and rupture stress σ_u of the bulk material of aluminium alloys and the machining affected layer produced in finishing conditions are the same. Therefore, the crack will initiate at the point where the local stress is the highest.

In contrast to previous works [5-7], the proposed model now includes the effect of surface topography and RS induced by machining to calculate the stress state. The effect of surface topography is computed using the stress concentration factor Kt, which can be calculated applying the approach developed in [9] to surface topography measurements. It should be noted that the effect of Kt is surface sensitive since it reaches ~10 µm in depth [10]. Consequently, the stress state beneath the surface only depends on the applied stress and RS field.

Fig. 1 shows a schematic of the proposed model. This model superimposes the effect of RS, surface topography and applied stress (Fig. 1a) to determine the stress state of the workpiece (Fig. 1b).

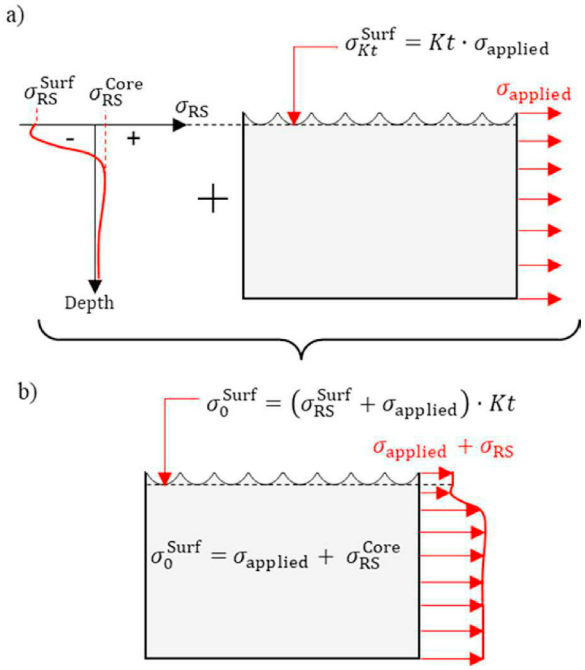

Fig. 1. Schematic of the fatigue initiation site prediction model. (a) superposition of the effect of RS and topography, b) resultant stress field.

The effect of surface topography on surface stresses ($\sigma_{Kt}^{\mathrm{Surf}}$) is calculated using eq. (1), where the applied stress $\sigma_{\mathrm{applied}}$ is multiplied by the stress concentration factor Kt at every point of the surface. Surface residual stresses $\sigma_{\mathrm{RS}}^{\mathrm{Surf}}$ must be added to determine the local stresses σ_0^{Surf}at the surface employing eq. (2). It should be clarified that in the present work the RS are assumed to be uniform since we only measured the RS at the center of the specimens. In the future, the model could be improved by adding numerically predicted RS across the entire surface or RS maps non-destructively measured by X-ray diffraction. Similarly, the local stress state within the core σ_0^{Core} is calculated by eq. (3), adding the applied stress and residual stresses $\sigma_{\mathrm{RS}}^{\mathrm{Core}}$ locked in the core.

$$\sigma_{Kt}^{\mathrm{Surf}}(x,y) = Kt(x,y) \cdot \sigma_{\mathrm{applied}} \quad (1)$$

$$\sigma_0^{\mathrm{Surf}} = \left(\sigma_{\mathrm{applied}} + \sigma_{\mathrm{RS}}^{\mathrm{Surf}}\right) \cdot Kt \quad (2)$$

$$\sigma_0^{\mathrm{Core}} = \sigma_{\mathrm{applied}} + \sigma_{\mathrm{RS}}^{\mathrm{Core}} \quad (3)$$

To identify the crack initiation site, local surface stresses (σ_0^{Surf}) and local stresses within the workpiece ($\sigma_{\mathrm{RS}}^{\mathrm{Core}}$) are compared. As previously explained, assuming that the yield stress σ_y and rupture stress σ_u are uniform from the surface to the bulk, cracks will be initiated at the surface if $\sigma_0^{\mathrm{Surf}} > \sigma_0^{\mathrm{Core}}$, exactly at the point with maximum *Kt*. On contrary, if $\sigma_0^{\mathrm{Surf}} < \sigma_0^{\mathrm{Core}}$ cracks will be initiated beneath the surface, at the point with highest tensile RS when the applied stress is constant across the section.

3. Materials and experiments

To validate the model, flat fatigue specimens were obtained from an aluminium 7050-T7451 prismatic bar with dimensions 400×100×40 mm. The mechanical properties of the raw material were determined by standard tensile tests (ISO 6892) and these are shown in Table 1, where *E* is Young's modulus, *v* is Poisson's coefficient, σ_y is the yield stress, σ_u is the rupture stress and *H* is the hardening modulus. The geometry of the fatigue specimens was designed according to ASTM E466-96 standard (see Fig. 2). It should be clarified that both ends of the fatigue specimen included holes to enable the clamping of the specimen to the CNC milling table used in the specimen finishing process.

Table 1. Mechanical properties of aluminium A 7050-T7451

E [GPa]	*v* [-]	σ_y [MPa]	σ_u [MPa]	*H* [MPa]
71	0.33	475	574	1645

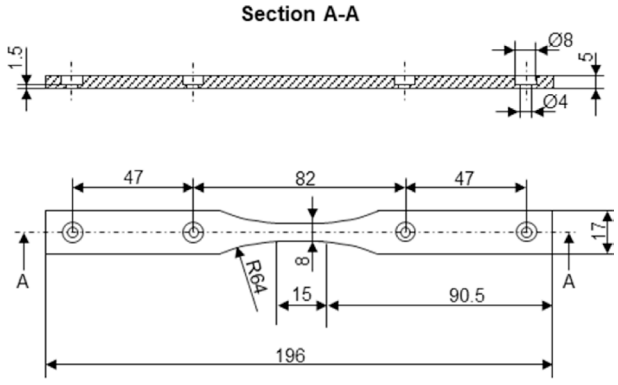

Fig. 2. Geometry of the fatigue specimen

To produce the fatigue specimens, firstly 200×18×6 mm flat samples were cut from the prismatic bar using a high precision saw. Then, the sides of the specimens were contour milled using smooth conditions, and the four holes were made at both ends (Fig. 2). The target surfaces for this study were the upper and bottom faces. These surfaces were faced milled using an indexable face milling cutter AF 730M D050 with a diameter of 50 mm with five uncoated inserts (APKT1604PDR X24CI10D). The characteristics of the insert are shown in Table 2. The specimen was fixed to the machine table using screws through the holes located at the ends of the specimen. The upper and bottom surfaces were face milled at cutting speed v_c = 200 m/min, feed per tooth f_z = 0.2 mm/tooth and depth of cut a_p = 0.5 mm, using a Minimum Quantity of Lubricant (MQL) supply. Finally, the edges of the specimen were manually ground using a 400-grit size sandpaper, to prevent from edge effects during fatigue tests.

Table 2. Characteristics of the APKT1604PDR X24CI10D inserts

Material	Rake angle [°]	Clearance angle [°]	Nore radius [mm]	Edge radius [µm]
Uncoated WC-Co	11	8	0.2	12-18

Although the same machining conditions were used to face mill the upper and bottom surface, chatter was generated in some surfaces when face milling the bottom surface. Since chatter leads to a rougher surface finishing, it is more likely to initiate a fatigue crack at this surface. Based on this assumption, only the residual stresses and topography of the bottom surface of the fatigue specimens was characterised.

The RS generated by the face milling process at the centre of the specimen were measured following the procedure given in the ASTM-E357 standard. Since finishing operations induce very shallow RS profiles, the fine increment hole drilling procedure developed by Grant et al. [11] was used to accurately measure RS changes from the surface to the bulk. The surfaces were prepared for gauge installation following the instructions of the gauge supplier. The smallest EA-06-031RE-120 strain gauges supplied by Vishay Measurement Group were bonded at the centre of the specimen after careful surface preparation. A Restan MTS3000 machine equipped with a high speed air turbine was used. The 0.8 mm diameter drill bit was aligned with the gauge before drilling the hole. The zero depth was detected by electrical contact between the drill bit and the specimen surface. Then, the incremental hole drilling procedure was conducted applying a total of 15 depth increments: five initial increments of 10 µm, subsequent five increments were of 20 µm, and the final five increments had a depth of 50 µm. This procedure generated a hole with a ≈ 0.9 mm diameter and a depth of 500 µm. Strains were recorded in a HBM data acquisition system after each increment. Finally, the procedure described in the ASTM-E357 was used to calculate the RS profiles. It should be noted that three specimens were used to characterise the RS but these were not used in the fatigue tests since the measurement process was destructive.

The surface topography of the specimens was measured using the confocal profilometer Alicona Infinite Focus IFG4 with the set-up shown in Fig. 3. Since we aimed at measuring the entire surface of the gauge region of the fatigue specimen, and this can require excessive time and generate significant amount of data, different measurement parameters were tested to find a balance between accuracy and time, by comparing roughness measurements *Ra*, *Rz*, and *Rq* determined with a contact roughness tester Mitutoyo Surftest SJ-210. Then, the surface topography of three fatigue specimens was characterised to validate the proposed model. Furthermore, preliminary observations showed that the bottom surface closer to the edges was rougher. To further reduce the surface topography characterisation process, two regions of 15×2 mm were analysed, named IR and IL in Fig. 3c. The parameters used in the confocal microscope were: 20× optical

magnification, lateral resolution of 50 nm and a vertical resolution of 2 µm.

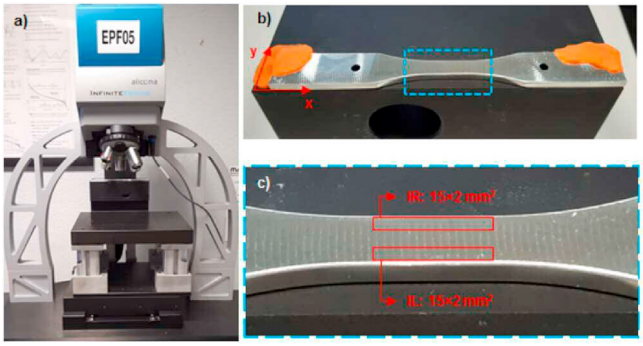

Fig. 3. a) Set-up used to measure surface topography, b) specimen orientation and c) identification of the characterised regions IR and IL

Uniaxial fatigue tests were done in a servohidraulic MTS 810 machine under load control at 10 Hz frequency and loading ratio R=0.1. To define the maximum load for the validation tests, calculations were done using the proposed model and the results from the RS measurements and surface topography analysis. Face milling induced compressive RS within the affected layer, and the surface RS had an average value of -230 ± 25 MPa in the longitudinal direction, and a maximum tensile RS of 32 MPa beneath the surface (see Fig.4). The stress concentration factor Kt in the loading direction was determined using the approach described in [9]. This showed values ranging from 5.2 to 9.8. To ensure that cracks were nucleated at the surface of all tested specimens for the validation, the minimum value of Kt = 5.2 was used in the calculations. The condition $\sigma_0^{\text{Surf}} > \sigma_0^{\text{Core}}$ was applied by combining eq. 2 and 3, leading to eq. 4. Then, we solved $\sigma_{\text{applied}} > 292$ MPa. Considering the uncertainty of experimental tests, fatigue tests were done with a maximum applied stress of 350 MPa to ensure that cracks were nucleated at the surface. Three specimens were tested.

$$\left(\sigma_{\text{applied}} + \sigma_{\text{RS}}^{\text{Surf}}\right) \cdot Kt > \sigma_{\text{applied}} + \sigma_{\text{RS}}^{\text{Core}} \quad (4)$$

Finally, the fracture of the tested specimens was observed using a microscope Leica DMS 1000 with depth of field correction.

4. Results and discussion

4.1. Residual stresses

Fig. 4 shows the average RS profiles measured on the face milled surfaces. As mentioned, these were measured on the bottom surface. Compressive RS were induced within 175 µm depth, and then slightly tensile RS were generated in the bulk material. Surface RS were similar in the longitudinal (x) and transverse direction (y).

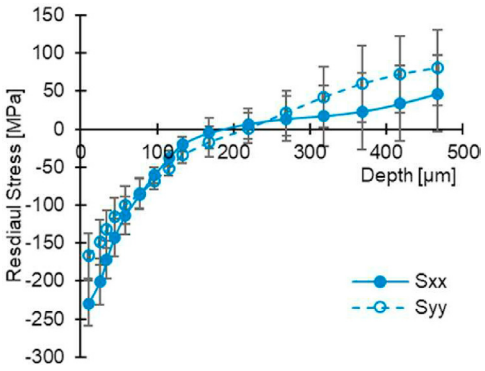

Fig. 4. Residual stress profiles induced by face milling

4.2. Surface topography

As described in the methodology, the topography of the three fatigue specimens was measured in two regions named IL and IR (see Fig. 3) and was postprocessed using the analytical approach described in [9] to obtain stress concentration factors in the loading direction (x). This analysis revealed IL region being more critical for specimens I and II, but region IR for specimen III.

Fig. 5, 6 and 7 show the surface topography results and calculated stress concentration factors for the most critical region of the three tested specimens. It is evident from the surface topography results that the distance between peaks is higher than the feed rate of 0.2 mm/tooth. This occurred because one insert was mounted at a lower position that the rest of inserts in the indexable tool. Consequently, the face milling was basically done by one insert. Specimen I showed a smoother surface topography because there was no chatter during its machining, but it is possible to observe the effect of chatter in specimens II and III since the topography does not follow a regular pattern.

The stress concentration distributions of the three samples show that Kt is below 2 almost across the entire surface, but peak stress concentration values are reached at very localised regions every tool pass. The maximum stress concentration factors of each specimen are identified in Fig. 5 to 7. Specimen I had a maximum Kt of 7.8, specimen III a maximum of 8.2 and the worst topography was generated in specimen II with a maximum Kt of 9.8.

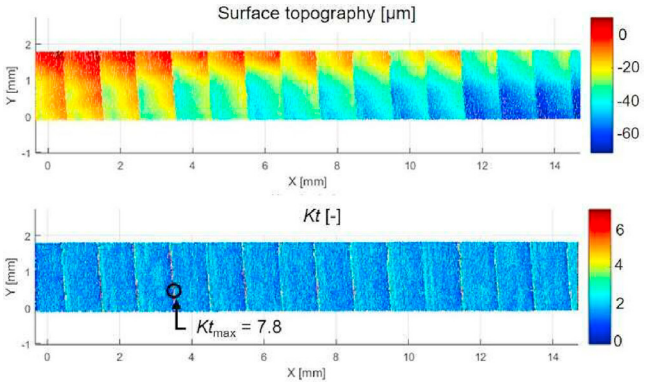

Fig. 5. Surface topography and stress concentration factor Kt in specimen I

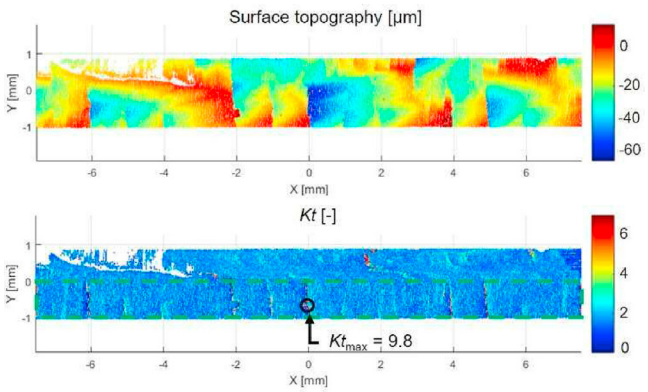

Fig. 6. Surface topography and stress concentration factor *Kt* in specimen II

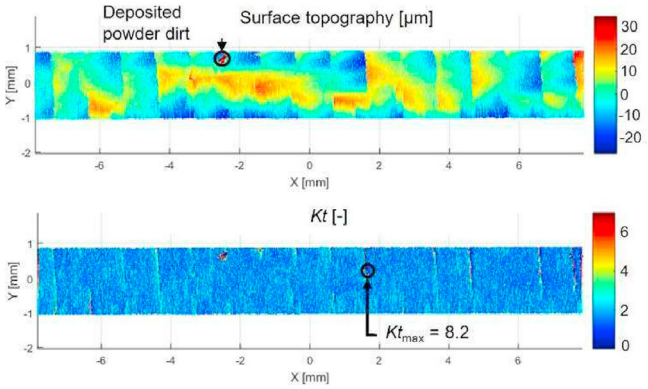

Fig. 7. Surface topography and stress concentration factor *Kt* in specimen III

4.3. Fatigue

Table 3 summarises the results of the fatigue tests. The fractography analysis confirmed that the cracks were nucleated at the flat surface of the specimens as predicted by the model. As expected, specimen I had the highest fatigue life because its maximum stress concentration factor (Kt_{max}) was the lowest among the tested specimens. Specimen III also showed a similar fatigue life (N_f), but the postmorten analysis found that fracture was out of the gauge region; it was localised in the transition radius. Specimen II with a stress concentration factor 25% higher than specimen I showed the shortest fatigue life, almost 50% shorter.

Table 3. Maximum stress concentration factors and fatigue results

Specimen	Kt_{max}	N_f [cycles]	Position of fracture
I	7.8	37027	Surface-Gauge region
II	9.8	18999	Surface-Gauge region
III	8.2	34660	Surface-Out Gauge region

The proposed model predicted that when the applied stress is $\sigma_{applied}$ >290 MPa, the fractures would start at the surface. The tests were done at slightly higher maximum applied stress ($\sigma_{applied}$ = 350 MPa), and the fatigue life ranged from ~19000 to 37000 cycles. Hence, the effect of surface topography under tested conditions (high values of stress concentration factor and compressive surface RS) seems to be only dominant close to the low cycle fatigue (LCF) regime. These results also show that despite being specimens manufactured at the same conditions, fatigue life can vary significantly for the same loading condition. Although not include in this work, we did additional tests below a maximum applied stress of 250 MPa and cracks were not nucleated in the face milled surface, which suggests that the compressive RS field prevents crack initiation near the surface and impacts on the high cycle fatigue strength of the material.

For further validation of the model, the exact point of crack initiation was compared to the location identified by the model. Specimen III was not considered in this analysis because its fracture occurred out of the gauge region of the specimen. Fig. 8 and 9 show the top surface and cross section of the fractured specimens.

Since cracks were initiated at the surface, eq. 2 of the proposed model was applied to calculate the distribution of surface stresses σ_0^{Surf} across the surface. The maximum stress concentrations of the tested specimens were very high (Kt >7.8) and calculated σ_0^{Surf} exceeded the yield stress σ_y of the material. Therefore, for a more accurate analysis of the surface stresses, these were corrected. Firstly, the equivalent Von Mises elastic stress σ_{VM}^{elast} was determined using eq. 5 for the distribution of stresses calculated following the elastic approach. If the equivalent Von Mises elastic stress σ_{VM}^{elast} was higher than the yield stress, the elastically calculated surface stresses needed to be corrected. To this end, Neuber's approach was used [12]. This assumes that the deformation energy determined using the elastic behaviour of the material is equal to the deformation energy obtained employing the elastoplastic behaviour of the material. Applying this concept, surface longitudinal stresses of plastically deformed points can be calculated using eq. 5 to eq.7.

$$\sigma_{VM}^{elast} = \sqrt{(\sigma_0^{Surf})^2 + (\sigma_{yy})^2 - \sigma_{yy} \cdot \sigma_0^{Surf}} \quad (5)$$

$$\sigma_{xx}^{plast} = \frac{\sigma_{yy} + \sqrt{4 \cdot (\sigma_{VM}^{plast})^2 - 3 \cdot (\sigma_{yy})^2}}{2} \quad (6)$$

$$\sigma_{VM}^{plast} = \sqrt{\frac{H \cdot (\sigma_{VM}^{elast})^2 + E \cdot (\sigma_{yy})^2}{H+E}} \quad (7)$$

On the bottom of Fig. 8 and 9 the longitudinal stresses corrected following the elastoplastic model can be observed. In both figures the maximum stresses are identified with black circles. It can be seen that they were close to the rupture stress of the material (574 MPa), and therefore explain the earlier crack initiation and LCF behaviour. Once having calculated the position of the maximum stress, this was compared to the experimentally observed crack initiation site. It should be noted that this step is not straightforward. The fatigue specimen underwent plastic deformation and therefore the dimensions of the specimens were modified with respect to its original size which is used in the analytical model. Thus, the final length of the fatigue specimen was measured and compared to the initial length, to determine a correlation factor to correct the coordinates for better comparison.

Interestingly, this analysis showed that the crack of specimen II was initiated at the position determined by the model (Fig. 9). The crack of specimen I was initiated at a different point, but importantly it also matched with one of the feed marks that led to high stress concentration confirming the

relevance of surface topography (Fig. 8). This encourages the use of stress concentration factor to analyse the effect of machining on fatigue performance, instead of using standard roughness parameters such as average arithmetic roughness *Ra* or peak to valley roughness *Rz* to correlate with fatigue performance. It should be noted that the model predicted a maximum stress of 561 MPa in specimen I, and the stress at the experimentally identified crack initiation site was only 16 MPa lower (2.8%), which could explain a reasonable uncertainty of the method. Multiple crack sites are also expected at high applied stresses (LCF regime), which could have contributed to the deviations with respect to the model.

The results confirm that the model can predict the crack initiation site. In future work, this model will be combined with a crack-propagation model that considers the properties of the machining-affected layer and bulk material. This will allow us to predict the fatigue life of machined components. Furthermore, it could be used to identify the target surface integrity properties to accomplish the required fatigue life.

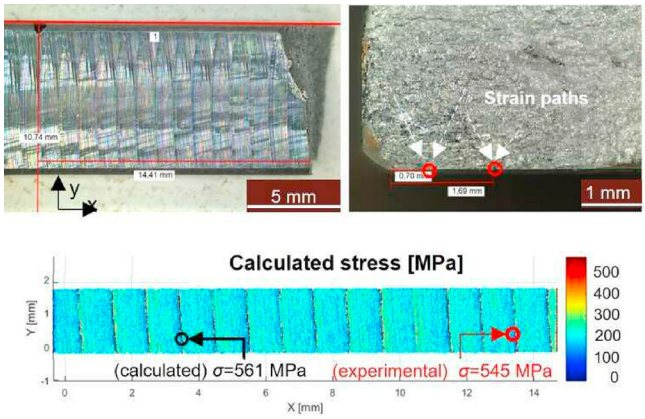

Fig. 8. Top view of the broken specimen I, fracture surface and longitudinal stress distribution when applying 350 MPa stress in the longitudinal direction

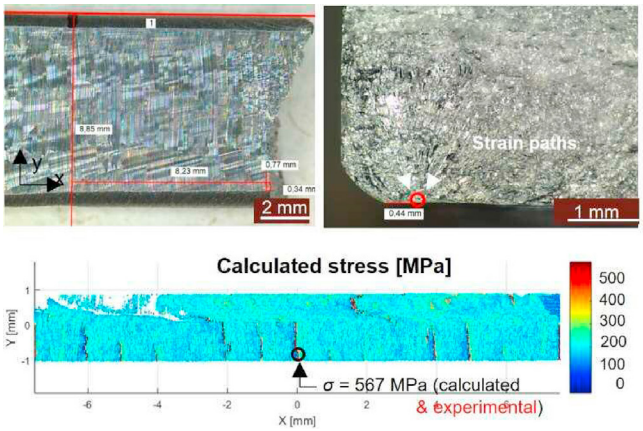

Fig. 9. Top view of the broken specimen II, fracture surface and longitudinal stress distribution when applying 350 MPa stress in the longitudinal direction

5. Conclusions

This paper proposes an analytical model to determine the fatigue crack initiation site in machined aluminium alloy components, considering the effect of surface topography and residual stresses. The main conclusions are:

- The model can identify the applied stress that induces cracks at the surface or beneath the surface. This depends on the effect of surface topography (stress concentration factor) and residual stress state.
- (Sub)surface compressive residual stresses induced by face milling operations prevent the initiation of cracks at the surface in the high cycle fatigue regime even if surface quality is rough (high values of stress concentration factor).
- Tests done at high applied stresses, where the surface topography is dominant, confirmed that cracks are nucleated at high stress concentration regions. Thus, instead of using standard roughness parameters, the stress concentration factor should be determined in fatigue analysis. Furthermore, local elastic stresses must be corrected under such conditions because the yield stress is exceeded in the critical regions.

Acknowledgements

The authors thank the Basque Government for the financial support given to the project FRONTIERS 2022 - *Superficies multifuncionales en la frontera del conocimiento* (KK-2022/00109). The authors would like to thank Denis Soriano for the technical assistance during machining tests.

References

[1] Fridlyander IN. Aluminum Alloys in Aircraft in the Periods of 1970–2000 and 2001–2015. Metal Sci Heat Treat 2001: 43(1):6-10
[2] Perez I, Madariaga A, Cuesta M, Garay A, Arrazola PJ, Ruiz JJ, Rubio FJ, Sanchez R. Effect of cutting speed on the surface integrity of face milled 7050-T7451 aluminium workpieces. Procedia Cirp 71 2018: 460-465
[3] Li LG, Wang SQ. Distortion caused by residual stresses in machining aeronautical aluminum alloy parts: recent advances. Int J Adv Manuf Technol 2017; 89(1):997-1012
[4] Ås S, Skallerud B, Tveiten B, Holme B. Fatigue life prediction of machined components using finite element analysis of surface topography. Int J Fatigue 2005;27(10–12):1590–6
[5] Suraratchai M, Limido J, Mabru C, Chieragatti R. Modelling the influence of machined surface roughness on the fatigue life of aluminium alloy. Int J Fatigue 2008;30(12):2119-2126
[6] Abroug F, Pessard E, Germain G, Morel F, Chové E. The effect of machining defects on the fatigue behaviour of the Al7050 alloy. Thirteenth International Conference on High Speed Machining 2016, Metz, France.
[7] Abroug F, Pessard E, Germain G, Morel F. A probabilistic approach to study the effect of machined surface states on HCF behavior of a AA7050 alloy. Int J Fatigue 2018; 116:473–489
[8] Madariaga A, Cuesta M, Dominguez E, Garay A, Ortiz-de-Zarate G, Arrazola PJ. Enhancing surface integrity of A7050-T7451 aluminium alloy by pneumatic machine hammer peening. Procedia CIRP 2022;108:317-322
[9] Perez I, Madariaga A, Arrazola PJ, Cuesta M, Soriano D. An analytical approach to calculate stress concentration factors of machined surfaces. Int J Mech Sci 2021;190:106040
[10] Zabala A, Blunt L, Tato W, Aginagalde A, Gomez X, Llavori I. The use of areal surface topography characterisation in relation to fatigue performance. In MATEC Web of Conferences, EDP Sciences, 2018;165:14013
[11] Grant P, Lord J, Whitehead P, Fry AT. The application of fine increment hole drilling for measuring machin-ing-induced residual stresses. Appl Mech Mater 2005;3:105-11
[12] Neuber H. Theory of stress concentration for shear-strained prismatical bodies with arbitrary nonlinear stress-strain law. J Appl Mech Trans ASME 1960;28(4):544–55